THE JOURNAL OF PHYSICAL CHEMISTRY C

Article

pubs.acs.org/JPCC

Molecular Orientation of Neurotensin and Its Single-Site Mutants on a Colloidal Silver Surface: SERS Studies

Prompong Pienpinijtham,[†] Edyta Proniewicz,*[,‡] Younkyoo Kim,[§] Yukihiro Ozaki,[†] John R. Lombardi,[⊥] and Leonard M. Proniewicz[†,‡,¶]

[†]Department of Chemistry, School of Science and Technology, Kwansei-Gakuin University, 2-1 Gakuen, Sanda, Hyogo 669-1337, Japan

[‡]Faculty of Chemistry, Jagiellonian University, ul. Ingardena 3, 30-060 Krakow, Poland

[§]Department of Chemistry, Hankuk University of Foreign Studies, Yongin, Kyunggi-Do, 449-791, Korea

[⊥]Department of Chemistry, City College of New York, 160 Convent Avenue, New York 10031, United States

[¶]The State Higher Vocational School, ul. Mickiewicza 8, 33-100 Tarnów, Poland

ABSTRACT: In this report, we describe a comprehensive systematic surface-enhanced Raman spectroscopy (SERS) study of the structures of neurotensin (NT), which is known to stimulate the growth of human tumors, in an aqueous solution of nanometer-sized colloidal silver particles under various environmental conditions, including excitation wavelengths (488.0, 514.5, and 785.0 nm), peptide concentrations (10^{-4}–10^{-6} M), pH levels of the solutions (from pH 2 to 11), H_2O/D_2O solvent exchange conditions, and structural mutations. The investigated mutated-NT analogues contain a natural (pig and frog NTs) and single-site synthetic ([Gln^4]-NT, [Trp^{11}]NT, and [D-Tyr^{11}]NT) backbone and/or side-chain modifications, which induce striking biological in vitro effects. On the basis of the analyses of the spectral profiles, specific conclusions were drawn with respect to the peptide geometry and changes in the geometry that occurred when the adsorption conditions were varied. In addition, the findings for adsorbed NT at different pH of silver sol were fully supported by a generalized two-dimensional correlation analysis (G2DCA).

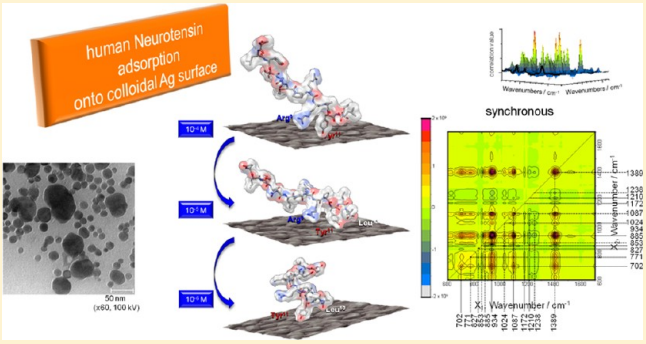

INTRODUCTION

Neurotensin (NT, pGlu^1-Leu^2-Tyr^3-Glu^4-Asn^5-Lys^6-Pro^7-Arg^8-Arg^9-Pro^{10}-Tyr^{11}-Ile^{12}-Leu^{13}OH, where pGlu represents 5-oxo-proline, and all amino acids are in the L-isomer) is a tridecapeptide that was first discovered, extracted, and sequenced from bovine hypothalami by Carraway and Leeman in 1973.[1,2] NT mediates the biological activity of NTR1 (neurotensin subtype-1 G-protein-coupled single seven-trans-membrane domain) regulatory receptors,[1,3] the overexpression and oversecretion of which are the signatures of cancers, such as pancreatic, colon, breast, prostate, and small cell lung cancers, pituitary adenocarcinomas, Ewing's sarcoma, and meningiomas.[4,5] The growth of tumor cells and other neoplastic cells is stimulated by the overexpression and oversecretion of NTR1.[6] Due to the poor expression or the absence of these receptors in normal cells, NTR1 receptors have been proposed as new tumor markers.[7,8] Understanding the underlying NT mechanisms would open tremendous opportunities for designing and developing drugs for controlling NTR1 receptor expression or disease progression and for the use of prognostic and predictive probes for tumor imaging.

As previously mentioned, NT plays an essential role in NTR1 biological activity. However, the detailed interactions involved in this activity are still unclear. Therefore, molecules based on *N*- and *C*-terminal fragments of the first NT analogues have been extensively studied.[9−11] The *N*-terminal end was found to contribute weakly to NT biological activity, whereas the binding occurs via so-called "receptor" sites, which relate to the *C*-terminal region of NT. However, the cleavage at the 8−9 amide bond can be prevented by the modification of the *N*-terminus.[12] The active fragment, which illustrates the pharmacological and/or biological effects of the full-length NT and has a high affinity to interact with NTR1, is composed of six residues at the *C*-terminal part in the sequence, which is known as the NT$^{8-13}$ hexapeptide.[13−15] For a shorter *C*-terminal fragment, such as NT$^{9-13}$ pentapeptide, the binding potency is dramatically decreased, which suggests that L-arginine at the 8 position (Arg^8) is important for binding.[16] The loss of binding potency of NT$^{1-12}$ dodecapeptide indicates the essential role of the Leu^{13}COOH terminus in NT activity.[17]

Received: May 1, 2012
Revised: July 12, 2012
Published: July 17, 2012

dx.doi.org/10.1021/jp304205d | J. Phys. Chem. C 2012, 116, 16561−16572

Table 1. Amino Acid Sequences of Human, Pig, and Frog Neurotensin and the Single-Site Mutants of Human Neurotensin, [Gln^4]NT, [Trp^{11}]NT, and [D-Tyr^{11}]NT

	amino acid sequence												
peptide	1[a]	2	3	4	5	6[a]	7	8[a]	9[a]	10[a]	11	12[a]	13[a]
NT	pGlu	Leu	Tyr	Glu	Asn	Lys	Pro	Arg	Arg	Pro	Tyr	Ile	LeuOH
[D-Tyr^{11}]NT	pGlu	Leu	Tyr	Glu	Asn	Lys	Pro	Arg	Arg	Pro	D-Tyr	Ile	LeuOH
pig NT	pGlu	Leu	Tyr	Glu	Asn	Lys	Ser	Arg	Arg	Pro	Tyr	Ile	LeuOH
frog NT	pGlu	Ser	His	Ile	Ser	Lys	Ala	Arg	Arg	Pro	Tyr	Ile	LeuOH
[Gln^4]NT	pGlu	Leu	Tyr	Gln	Asn	Lys	Pro	Arg	Arg	Pro	Tyr	Ile	LeuOH
[Trp^{11}]NT	pGlu	Leu	Tyr	Glu	Asn	Lys	Pro	Arg	Arg	Pro	Trp	Ile	LeuOH

[a]Common amino acid in the sequence of all the investigated peptides.

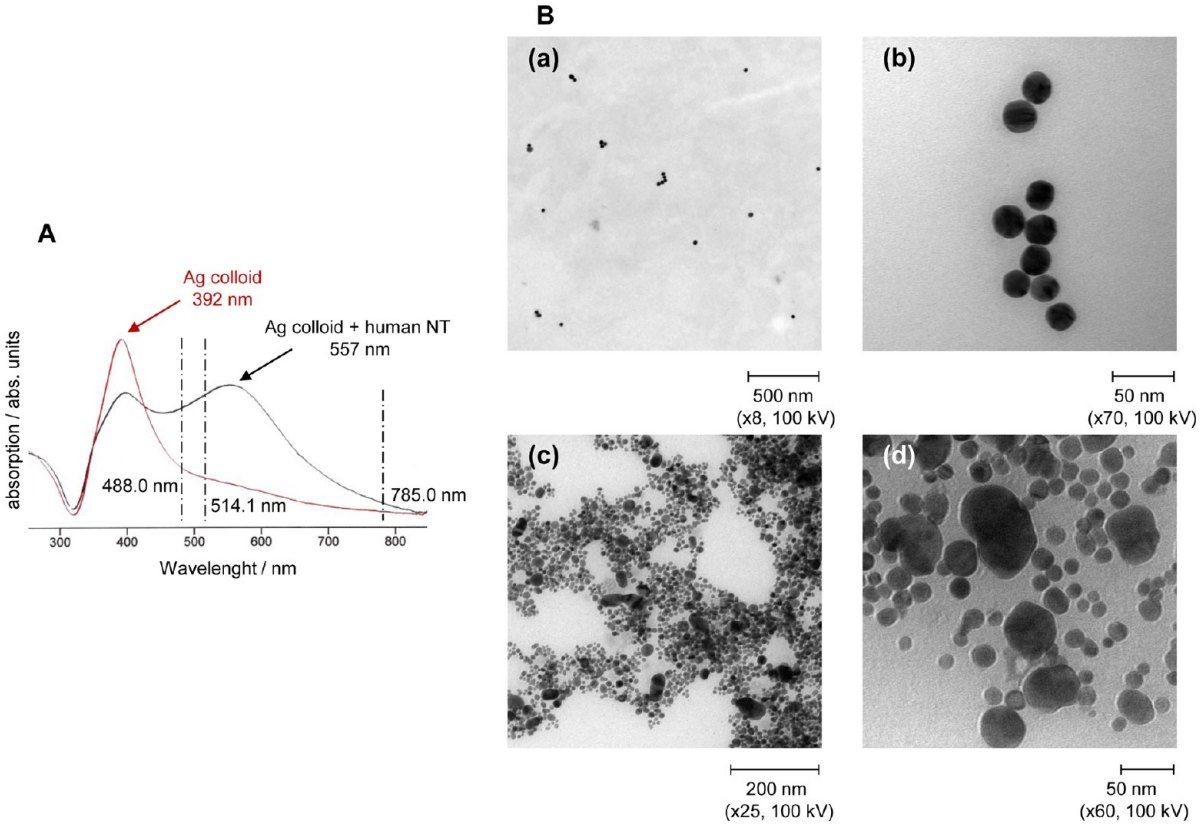

Figure 1. Excitation spectra (UV−vis) (A) and transmission electron microscopy (TEM) (B) images of a clear silver colloid used in this work (a and b images) and a peptide/Ag nanoparticles system (c and d images).

Furthermore, Tyr^{11} was demonstrated as a necessary amino acid in the NT interaction with NTR1.[14,18,19] Thus, the NT activity is altered by incorporation of a large spherical amino acid in the phenol side chain of Tyr^{11}. Nevertheless, the substitution of Try^{11} (or Tyr^3) with L-phenylalanine, which has no hydroxyl group, results in no difference in binding potency compared to NT.[17] In addition, the replacement of the residues pGlu^1 through Pro^7 with their corresponding D-isomers yields no effect on the binding of neurotensin.[17] The results of numerous NT$^{9-13}$ fragment studies have suggested that at least one basic residue is needed. The NT function to stimulate the formation of intracellular cyclic GMP requires the residues of Pro^{10} and Tyr^{11}.[18] The replacement of Arg^8 and Arg^9 residues with D-Arg and D-Lys, respectively, reduces NT agonistic properties, which is evidence of their importance in the receptor recognition function.[19]

In our previous works, we have systematically investigated the vibrational structure and the adsorption mechanism of bombesin (BN), BN analogues, and related peptides on Ag, Au, and Cu surfaces (at electrodes and/or in sol). We have also examined the changes in this adsorption process with respect to the applied electrode potential, the type of mutations in the BN amino acid sequence, the elongation of the BN C-terminal end, and small secondary-structure alterations for BN-related peptides.[20−28] The information obtained from SERS measurements was compared to the information regarding the contribution of the structural components of BN to their ability to interact with a bombesin-preferred GPCR. In each of these studies, we have demonstrated that the same amino acids (peptide fragments) that are responsible for the interaction with the SERS substrates are also involved in the interaction with the receptors. In addition, we have shown that these peptide fragments, which have been suggested to lack a direct influence on the substrate−receptor binding, are not active in SERS. Moreover, we have shown that during binding to the Ag surface, bombesin changes its secondary structure from random

dx.doi.org/10.1021/jp304205d | J. Phys. Chem. C 2012, 116, 16561−16572

to a β-sheet with a turn at the Val-Gly-His-Leu location, as is postulated for substrate−receptor binding.[29] We have shown that the mechanism for the adsorption of the studied compounds depends strictly upon the substrate properties (colloid vs electrode), which yields a range of possible binding conformers. This range of conformers, in turn, allows us to identify the most active molecular fragments involved in the adsorption at the solid/solution interface.

Because of the aforementioned interesting findings, we have recently compared data from biological activity studies with those from SERS studies for pig, frog, and human neurotensins for specifically mutated human analogues and fragments of NT deposited onto an electrochemically roughened silver substrate.[30−32] In this report, we present an in-depth description of the mode of adsorption of NT in an aqueous silver sol under different environmental conditions, including excitation wavelengths (488.0, 514.5, and 785.0 nm), peptide concentrations (10^{-4}−10^{-6} M), pH levels of the solutions (from pH 2 to 11), H_2O/D_2O solvent exchange conditions, and structural mutations. The investigated mutated peptides constitute a group that contains a natural (pig and frog NTs) and single-site synthetic ([Gln^4]NT, [Trp^{11}]NT, and [D-Tyr^{11}]NT) series of backbone and/or side-chain modifications, which induce striking biological in vitro effects. Table 1 presents the amino acid sequences of these neuropeptides. The purpose of this work is to elucidate the adsorption mode (the influence of structural modifications and environmental conditions) of neurotensin in the silver sol. This understanding allows for future predictions regarding the interaction between a peptide of a known amino acid sequence and a given silver surface. We expect that the SERS-active molecular fragments will also be biologically active at the NTR1 receptor binding site. Under this assumption, the results obtained during this work provide an understanding of the specificity of the binding of NT to the NTR1 receptor, which is not currently available.

EXPERIMENTAL SECTION

Neurotransmitters. Human, pig, and frog neurotensins, and single-site mutants of human neurotensin, [Gln^4]NT, [Trp^{11}]NT, and [D-Tyr^{11}]NT, were purchased from Bachem (Switzerland). Their purity and chemical structures were determined by using ^{1}H and ^{13}C NMR spectroscopy (Bruker Avance DRX 300 MHz spectrometer) and electrospray mass spectrometry (Finnigan Mat TSQ 700).

SERS Measurements. SERS spectra were recorded in silver colloidal dispersions. Silver colloidal dispersions prepared by simple borohydride reduction of silver nitrate were used as substrates. Figure 1 provides an overview of the morphology of the substrates used in this work.

$AgNO_3$ and $NaBH_4$ were purchased from Wako (Japan) and used without further purification. Three batches of colloidal silver solutions were prepared according to the standard procedure.[33] Briefly, 42.5 mg of $AgNO_3$ dissolved in 50 mL of deionized water at 4 °C was added dropwise to 150 mL of 2 mM $NaBH_4$ immersed in an ice bath, while the mixture was stirred vigorously. After the addition of $AgNO_3$ was complete, the resulting dark-yellow solution was stirred continuously at 4 °C for approximately 1 h.

Batch aqueous sample solutions were prepared by dissolution of the sample in deionized water (18 MΩ cm). The final concentration of the sample after being mixed with the colloid was adjusted to 10^{-4} M . To investigate the effect of pH, the proper solution was prepared by dilution of 0.1 M HNO_3 or NaOH solutions with water until the desired pH was obtained. Ten microliters of 10^{-4} M peptide aqueous solution was mixed with 70 μL of pH solution for 5 min, and 20 μL of Ag nanoparticles was subsequently added to set the final concentration of peptide at 10^{-5} M and diluted 10 times. The mixture was kept for 15 min before the SERS measurement.

At the concentration of 10^{-5} M, we expect only partial coverage of a surface (less than a monolayer). To prove this hypothesis, we measured the SERS spectra for species adsorbed from a solution with a concentration 10 times more dilute and from a solution with a concentration 10 times more concentrated (appearance of monolayer/bilayer). No spectral changes that could be associated with sample decomposition or desorption processes were observed during these measurements.

The experiment in D_2O was performed by mixing 10 μL of peptide sample with 70 μL of D_2O for 30 min. Twenty microliters of Ag nanoparticles was added to the D_2O mixture, and the resulting mixture was allowed to settle for 15 min before the SERS measurement (peptide concentration 10^{-5} M).

All samples were transferred into a glass capillary and measured directly by using microscope objective (50×, Olympus).

The SERS spectra of the peptides were collected with a HoloSpec f/1.8i spectrograph (Kaiser Optical Systems) equipped with a liquid-nitrogen-cooled CCD detector (Princeton Instruments), and the 785 nm line of a NIR diode laser (Invictus) was used as an excitation source. For 514.5 and 488.0 nm excitation SERS measurements, a Raman spectrophotometer (model RS-2100, Photon Design) equipped with a charge-coupled device (CCD) (Princeton Instruments) was used with excitation wavelengths of 514.5 and 488.0 nm from an Ar^+-ion laser (Spectra Physics). A standard procedure was used to choose the best measurement conditions. Thus the laser power was varied from 1 to even 50 mW and several SERS spectra with different laser power and different accumulation time were checked for any changes to make sure that neither thermal degradation nor (possible) photodegradation nor desorption of the sample took place. On the basis of these earlier measurements in each experiment presented here the laser power at the sample was set at ∼15 mW (for all laser lines). The typical exposure time for each SERS measurement in this study was 20 s with eight accumulations.

Typically, the SERS spectra were measured at 8 spots on the surfaces of the colloidal silver nanoparticles and were recorded after 15 min of incubation with the silver colloid and within 1 h of sample addition to the silver sol. The spectra from the series were nearly identical (well reproducible), except for small differences (up to ∼5%) in some band intensities.

Transmission Electron Microscopy. A transmission electron microscope (TEM) from Hitachi High-Technologies, model H-7650, at an accelerating voltage of 100 kV was employed to collect TEM images of synthesized Ag nanoparticles and peptide/Ag nanoparticles.

Spectral Analysis. The spectral analysis presented in this work was performed with use of the GRAMS/AI 8.0 (Thermo Electron) software package.

Generalized Two-Dimensional Correlation Analysis. G2DCA of the SERS spectra of human NT adsorbed on the colloidal silver surface in an aqueous solution at a peptide concentration of 10^{-6} M was performed by using the software package SpectraCorr version 1.1 SP1 by Thermo Fisher

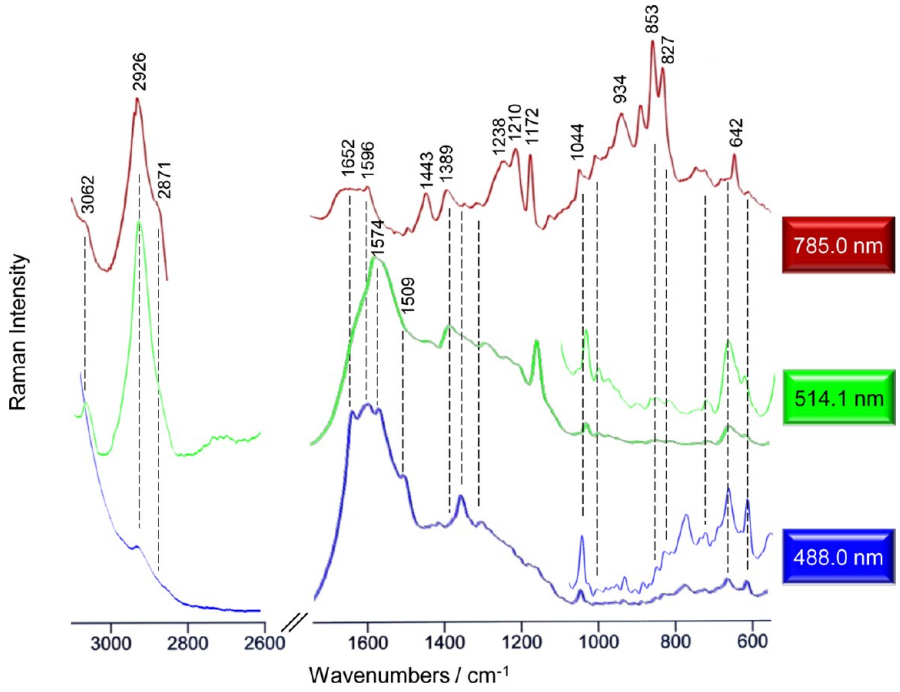

Figure 2. SERS spectra of human NT in an aqueous silver sol at pH 2 excited at 488.0, 514.1, and 785.0 nm in the spectral range of 3100−540 cm^{-1} (insets: spectra in the extended scale).

Scientific, 2004−2007. The G2D maps were generated by using changes in the pH of the aqueous solution as a perturbation variable. The original data set contains the five normalized pH-dependent SERS spectra. The original spectra were compared to a reference spectrum (average spectrum of the data set). By subtracting the reference spectrum, so-called dynamic spectra were calculated that formed the corresponding dynamic data set. Because real SERS spectra contain a certain level of noise, a noise filter coefficient of 0.08 with a global phase correlation of 0.2 was used.

RESULTS AND DISCUSSION

The addition of human NT (10 μL of 10^{-4} M) to silver colloid (20 μL) changed the color of the colloid from yellow to red. This color change resulted from aggregation of the colloid particles, as evidenced by the excitation spectra (UV−vis) (the surface plasmon band of these nanoparticles at 392 nm)[34] and the transmission electron microscopy (TEM) images at different magnifications (scale bars are from 500 to 50 nm) of the clear silver colloid and peptide/Ag nanoparticles system shown in Figure 1, parts A and B, respectively. The unaggregated colloid primarily contained silver spheres with diameters of approximately 20−25 nm (Figure 1, part B, panels a and b). Aggregation did not produce fusion into larger particles but rather assemblies of apparently randomly adhering spheres, each of which had dimensions approximately equal to the original dimensions (Figure 1, part B, panels c and d). These large assemblies are responsible for the color change (the metal particles become electronically coupled) that results from the broadness and red-shift to 557 nm of the plasmon resonance (Figure 1A). In this figure there is no evidence of charge-transfer transition that is required to explain results presented in Figure 2. However, as mentioned earlier, at this concentration of peptide, investigated molecules form a monolayer at most, thus this thin layer will result in a weak charge-transfer transition, which would be most likely overwhelmed by the tail of the UV−vis coagulation peak. That is why it is not clearly observed in this spectrum. The TEM images clearly show that the deposited peptide exhibits a sponge-like structure with a width/length in the range of 40−90 nm that covers the substrate surface (see Figure 1B, panel c) with a random distribution. Magnification of the panel c image in Figure 1B (see Figure 1B, panel d) shows that no identifiable form is apparent.

The SERS spectra of human neurotensin absorbed on the colloidal silver surface in an aqueous solution of pH 2 obtained with 785.0, 514.5, and 488.0 nm laser excitations are presented in Figure 2 (the vertical dashed lines in Figure 1A indicate the positions of these excitation lines). The relative intensities of the bands in these spectra strongly depend on the excitation wavelength as is expected for the resonance mechanism of enhancement. It has to be noted that bands observed in SERS spectra excited with the 488.0 and 514.5 nm laser lines are also present in the spectrum obtained upon 785 nm laser excitation. In addition in this last spectrum (785 nm excitation) there were additional bands that are not clearly observed in these other two. In particular, the SERS signals at 642, 827, 853, 885, 934, 1172, 1210, 1238, 1389, and 1443 cm^{-1} in the SERS spectrum obtained with 785.0 nm excitation were significantly strengthened compared to those obtained with the other two excitation wavelengths. This could be characteristic of an increase in vibronic coupling, often associated with the intervention of charge-transfer transitions.[35] On the other hand, there is no evidence of charge-transfer transition in Figure 1A. The peak at 557 nm in this figure is due to coagulation effects of the colloid. However, due to a rather low concentration of NT that forms a monolayer at most, this thin layer will result in a very weak charge-transfer transition, which would most likely be overwhelmed by the tail of the coagulation peak.

The SERS pattern of the aforementioned signals is similar to that observed for a variety of Tyr-containing peptides in which

dx.doi.org/10.1021/jp304205d | J. Phys. Chem. C 2012, 116, 16561−16572

Table 2. Wave Numbers and Band Assignments for SERS Spectra of Human, Pig, and Frog Neurotensin and [D-Tyr^{11}]NT, [Gln^{4}]NT, and [Trp^{11}]NT, the Single-Site Mutants of Human Neurotensin[a]

assignment	wavenumbers [cm^{-1}]					
	human NT	[D-Tyr^{11}] NT	[Gln^{4}] NT	frog NT	pig NT	[Trp^{11}] NT
$\nu(CH)_Y$	3062	3060	3065			3060
$\nu_{as}(CH)$	2926	2925	2929	2929	2926	2928
$\nu_s(CH)$	2871	2873	2868	2865	2870	2868
ν(ring) + $\rho_s(NH_2)$	1652	1668	1665	1631	1650	1626
$\nu(CC)_Y$		1612	1614			
W8a						1593
Y8a	1596	1596	1595	1606	1597	
Y8b		1574	1574	1576	1574	
Y19a	1491		1490			
W4 [ν(C═C)]						1503
Y19b/W6 [$\nu_s(N_1C_2C_3)$ + $\delta(N_1H)$ and $\delta(CH)_{phenyl}$] and $\rho_s(C_\beta H_2)_{Y,W}$	1443	1446	1445	1445	1447	1439
$\nu(C_\alpha OO^-)$	1389	1391	1390	1393	1389	1411
W7/$\delta_s(CH_2)$ and ν(C−X)				1366		1370
W7 [pyrrole $\nu(N_1C_8)$ + oop bending; Fermi resonance]						1356
$\nu(CC)_Y$ and/or $\rho_w(CH_2)$	1343	1333			1329	
$\nu(CC)_Y$, ν(CO), Y9a (ρ_{ipb}(CH)) $\nu(COH)_Y$, and $\rho_w(C_\beta H_2)_{Y,W}$	1309	1318	1317	1304	1319	
					1301	
amide III				1259		1275
$\nu(C-O)_Y/\nu(C-OH)_Y$ and $\rho_b(COH)_Y$	1238	1231	1225	1237	1226	
W10 ($\nu(C_3-C_{10})$)						1227
totally symmetric para-substituted benzene	1210	1212		1214		1212
ν_{sym} ($C_\beta C_\gamma H_2 C_\delta$)	1172	1173	1172	1175	1173	
$\delta(N_1H)$						1132
ν_{as}(CCN), $\rho_t(NH_2)$, and/or $\rho_w(CH)_{Y,W}$	1124	1119	1120	1128	1120	
$\nu(C-N)_R$	1085					1075
ν(C−C) and/or $\rho_r(C_\gamma H_2)$	1044	1045	1042	1046	1045	1050
W16 (breathing out-of-phase)						1006
Y	1003	997	1002	1002	1002	
ν_{as}(CCC) and $\rho_{oopw}(CH)_Y$					967	
$\nu_{sym}(C_\beta-C_\alpha OO^-)_L$	934	934	944	930	933	944
$\rho_r(C_\gamma H_2)_Y$	885	884	885	883	885	
ν(C−C)						866
ν(C−C) and ν_{as}(CNC)						835
Y doublet	853	853	853	856	853	
Y doublet	827	828	828	827	827	
$\delta(COO^-)_L$	807		806	806		
$\nu(CNH)_R$	781[b]					
W18						765
$\rho_b(ring)_Y$	741	741	741		741	
Y/W	719	720	718	718	719	718
ρ_{oopb}(ring)					679	671
δ(ring)	642	642	642	646	642	
amide V						633

[a]Abbreviations: Y, L, R, and W = tyrosine, leucine, arginine, and tryptophane residues, respectively; ν = stretching, δ = deformation, ρ_w = wagging, ρ_b = bending, ρ_t = twisting, ρ_r = rocking, ρ_s = scissoring, s = symmetric, as = antisymetric, oop = out-of-plane vibrations. [b]Observed at peptide concentration 10^{-4} M.

the Tyr residue is coordinated to a metal ion.[36−38] This behavior strongly implies that Tyr is adsorbed onto the colloidal silver surface. The proposed band assignments for these SERS signals based upon the approximation of C_{2v} symmetry of the para-substituted phenyl ring are given in Table 2, and the assignments agree with the extensive band assignments for human NT, its mutated fragments and analogues, and related peptides in the solid state and immobilized onto the electrochemically roughened silver substrate reported by Proniewicz and co-workers.[30−32] The assignments also agree with ground-state spectroscopy results of para-substituted phenyls[3940] and studies of Tyr and Tyr-containing peptides.[36−38] Similar spectral features were observed for excitation wavelengths in the green and blue bands. These features, except that at 1172 cm^{-1} (see Table 2 for band assignments), exhibit significantly lower relative intensities upon excitation at 514.5 and 488.0 nm. In contrast, the relative intensities of the 1652, 1596, and 1574 cm^{-1} SERS signals (see Table 2) increased for both of these excitation wavelengths. In addition, at 488.0-nm excitation, one more band at 1509 cm^{-1} (Y19a + $\nu(C-O)_Y$) increased in intensity. A comparable spectral feature has been detected for human NT

dx.doi.org/10.1021/jp304205d | J. Phys. Chem. C 2012, 116, 16561−16572

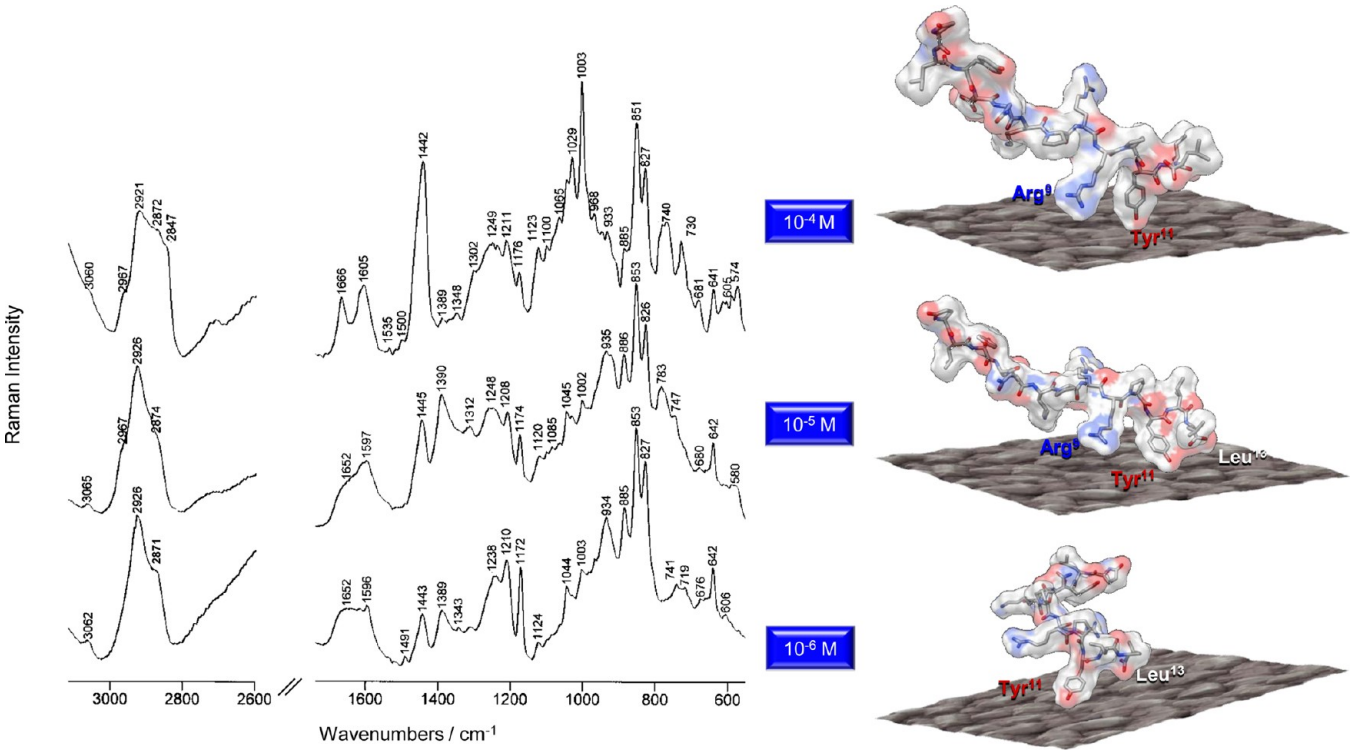

Figure 3. SERS spectra of human NT in an aqueous silver sol at pH 2 and at peptide concentrations of 10^{-4}, 10^{-5}, and 10^{-6} M in the spectral range of 3100−540 cm^{-1} and proposed reorientation of the Tyr ring of NT on the colloidal silver surface upon change of peptide concentration.

and its analogues immobilized onto the electrochemically roughened silver substrates,[30−32] for tyrosyl radicals studied in vitro,[41,42] for Tyr-containing peptides,[38,43] and for tyrosinate−metal biological complexes.[37]

By monitoring the excitation spectrum as a function of peptide concentration, we observed that the maximum aggregation occurred at a concentration of 10^{-4} M with no further increase at greater concentrations. This value was used as the optimal peptide concentration for monolayer colloidal coverage.[44] The influence of the concentration of human NT adsorbed onto the colloidal silver surface in an aqueous solution at pH 2 on the peptide SERS spectrum is illustrated in Figure 3. From this figure, the human NT SERS spectra for the peptide concentrations of 10^{-4}, 10^{-5}, and 10^{-6} M showed the same bands that originated mainly from the Tyr residue and the carboxylate and amino groups (see Table 2). These results suggest the model of peptide binding via these peptide fragments within the investigated concentration range. However, an increase (approximately 1389, 1172, 934, and 885 cm^{-1}) and decrease (approximately 1443, 1029, 1003, 781, and 740 cm^{-1}) (see Table 2 for band assignments) in the relative band intensities were noticeable according to peptide dilution. This behavior indicates the reorientation of the aforementioned peptide fragments onto the surface of the silver nanoparticles. On the basis of the results presented in Figure 3, the following general interpretation of the observed spectral changes upon concentration reduction of human NT was proposed based on the tendency of the Tyr SERS signal relative intensities (approximately 1443, 1029, 1003, and 740 cm^{-1}). At a concentration of 10^{-4} M the silver colloidal surface is packed with the peptide molecules with the Tyr ring being almost perpendicular to the surface. Such orientation is proved by observation of the strongly enhanced 1029 and 1003 cm^{-1} SERS features (see Table 2 for assignment). It is expected that such close packing is stabilized by π stacking of the Tyr phenyl rings of neighboring molecules. That these features decreased as the peptide concentration was decreased implies that the Tyr ring was leaning on the silver colloidal surface, which resulted in the strengthening of the interaction between the Tyr π-electron system and the silver surface. The increase of the silver surface coverage by the oriented nearly flat Tyr rings limited the interaction with the amine group of Arg (i.e., the band at 781 cm^{-1} diminished) (Figure 3, bottom trace), either through increasing distance from the surface of $-NH_2$ or via specific molecule reorientation, which placed the N−C bond in a position that is not preferred for interactions between the free electrons pair on the N atom and the silver surface. However, this orientation was favorable for the $-C_\alpha OO^-$ group and the Tyr $-C_\beta C_\gamma H_2 C_\delta-$, $C_\beta-C_\alpha$, and $-C_\gamma H_2-$ units adsorption onto the silver surface, which is manifested by the increase in I_{1390}, I_{1172}, I_{934}, and I_{885} (where I_X is SERS relative intensity of band X), respectively. In summary, the SERS spectrum at a peptide concentration of 10^{-5} M (Figure 3, middle trace) indicates that both the carboxylate and amino groups were in close proximity to the silver surface, which can be observed from the 1389 and 781 cm^{-1} bands corresponding to the $\nu(C_\alpha OO^-)$ and ν(CNH) modes, respectively. In contrast, the SERS spectra at peptide concentrations of 10^{-4} (Figure 3, top trace) and 10^{-6} M (Figure 3, bottom trace) indicate that only one of these groups, $-NH_2$ or $-C_\alpha OO^-$, respectively, interacted with the surface. Furthermore, from the lack of an observed O−H stretch, the phenolic group appears to have undergone deprotonation upon adsorption. In practice, for para-substituted benzenes, Tyr, and Tyr-containing peptide complexes, the phenolic hydrogen has been demonstrated to be lost during interaction with a metal.[37,43,45,46] This statement is supported by the substantial wavenumber lowering of Y8a at 1596 cm^{-1} ($\Delta_\nu = -17$ cm^{-1})[47] and the appearance of the 1652 and 1443 cm^{-1} bands.[43,46]

dx.doi.org/10.1021/jp304205d | J. Phys. Chem. C 2012, 116, 16561−16572

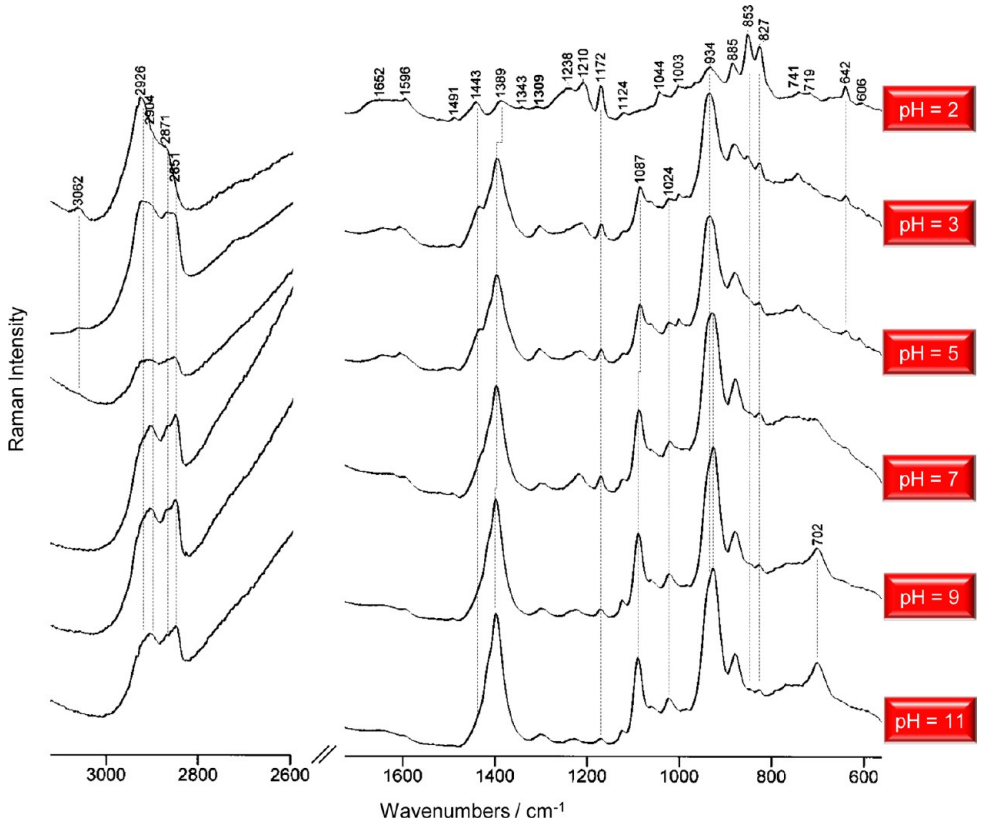

Figure 4. SERS spectra of human NT in an aqueous silver sol at pH values between 2 and 11 and at a peptide concentration of 10^{-6} M in the spectral range of 3100−540 cm^{-1}.

The Tyr ring, the Tyr $-C_\gamma H_2-$ moiety, the guanidine group of Arg, and the carboxylate group of *C*-terminal Leu interacted with the silver substrate and should therefore be located on the same side of the polypeptide backbone. As was evident from the solution structure of neurotensin in the membrane-mimetic environments,[48] only three positions in the sequence fit these requirements: 9, 11, and 13 (Arg^9, Tyr^{11}, and Leu^{13}). These residues interact with the silver substrate to constrain the rather rigid structure of the 9−13 *C*-terminal fragment, whereas the low affinity of the "binding sites" of the *N*-terminal fragment could be the consequence of a higher degree of exposure of the *N*-termini to the solvent.

The pH-dependent variations (from pH 2 to 11) in the SERS patterns of human NT deposited onto the silver nanoparticles in an aqueous solution at a peptide concentration of 10^{-6} M are presented in Figure 4. An examination of the spectra showed that in contrast to the previously discussed SERS spectrum of human NT (Figure 3, bottom trace), the SERS spectra at pH 3 and greater pH levels have almost identical spectral profiles that are dominated by the 1389 ($\nu(C_\alpha OO^-)$), 1087 (ν(C−N) of the guanido group), and 934 cm^{-1} ($\nu_{sym}(C_\beta-C_\alpha OO^-)$) spectral features. These spectral features indicate that the $-NH_2$ and $-C_\beta-C_\alpha OO^-$ groups are bound to the colloidal silver surface. However, these individual bands have different relative intensities because of the differences in the strength of the interactions between the $-NH_2$ and $-C_\beta-C_\alpha OO^-$ moieties and the substrate. To examine the magnitude of the changes in the relative band intensities changes upon an increase in the pH of the solution, a generalized two-dimensional correlation analysis (G2DCA) was applied. The G2D correlation method usually allows the distinguishing of spectral intensity changes that are not sufficiently pronounced to be observed by using simple visual spectral analysis. This method also allows for the observation of an increasing separation of the overlapping components presented within a broad band envelope. This method is useful in the analysis of spectral signals that change as numerous types of physical variables affect the spectra, such as time, temperature, pH, concentration, potential, pressure, conformation, and even chemical reaction.[27,49−51] Figure 5 represents the synchronous (parts A and C) and asynchronous (parts B and D) 2D correlation maps generated from the SERS spectra of human NT shown in Figure 4. The synchronous G2D correlation maps for human NT (Figure 5, parts A and C) contain four strong autopeaks (at (1389, 1389), (1087, 1087), (934, 934), and (2851, 2851) cm^{-1}), one medium-strength autopeak (at (702, 702) cm^{-1}), and five low-intensity autopeaks (at (1024, 1024), (885, 885), (853, 853), (827, 827) and (771, 771) cm^{-1}). The magnitude of the intensity of these autopeaks provides information regarding the extent of the changes in the relative intensities with changes in pH. For example, the strong enhancement of the (1389, 1389), (1087, 1087), (934, 934), and (2851, 2851) cm^{-1} bands indicates significant strengthening at these wavenumbers with increased pH, whereas the relative intensity changes of the 885, 853, and 827 cm^{-1} bands can be neglected. In addition to the autopeaks, three pronounced intensities at (1389, 934), (1087, 934), and (1389, 1087) cm^{-1} and nine medium intensities at (934, 702), (934, 771), (934, 885), (1087, 702), (1087, 771), (1087, 885), (1389, 702), (1389, 771), and (1389, 885) cm^{-1} presented positive cross-peaks in the G2D synchronous correlation map. The positive sign of these cross-peaks indicates that all of these SERS signals underwent pH-dependent changes in the same

dx.doi.org/10.1021/jp304205d | J. Phys. Chem. C 2012, 116, 16561−16572

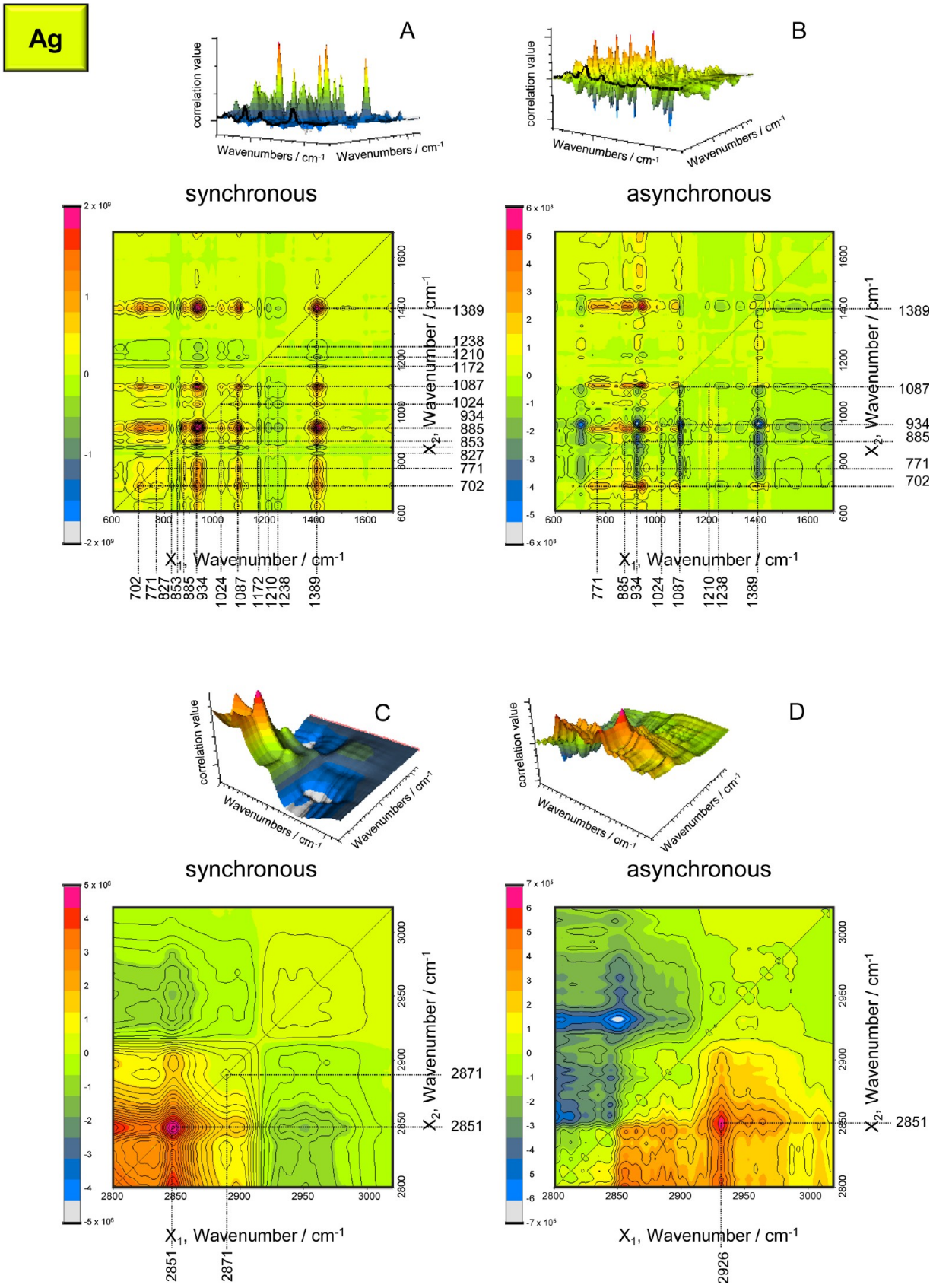

Figure 5. G2D synchronous (A and C) and asynchronous (B and D) correlation maps of the SERS spectra of human NT in an aqueous silver sol as a function of pH (2−11) of the solution; spectral ranges of parts A and B of 600−1700 cm^{-1} and parts C and D of 2800−3020 cm^{-1}; peptide concentration of 10^{-6} M.

dx.doi.org/10.1021/jp304205d | J. Phys. Chem. C 2012, 116, 16561−16572

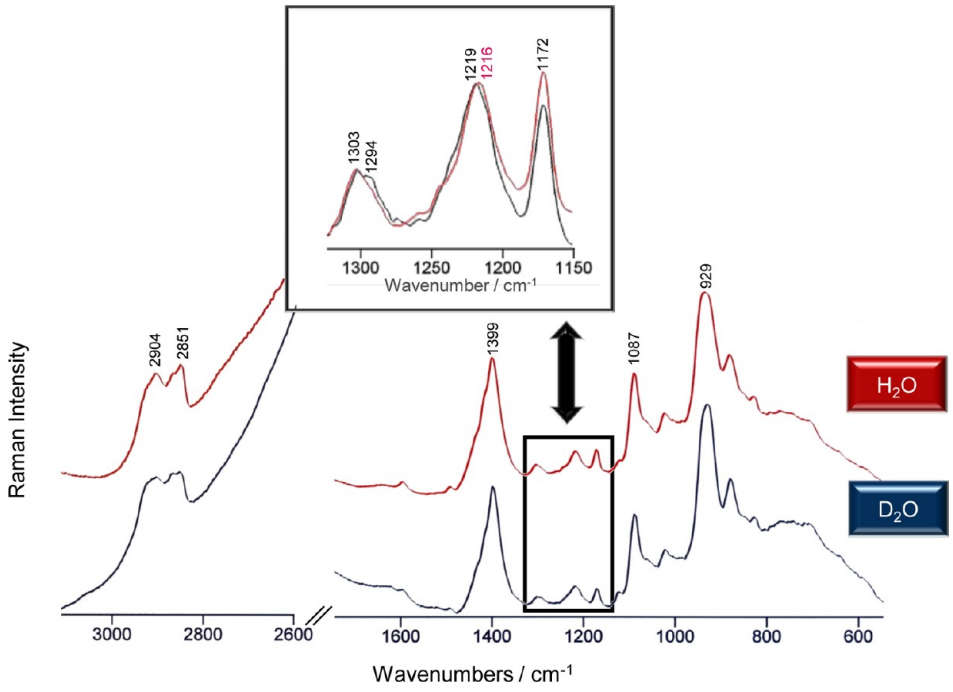

Figure 6. SERS spectra of human NT in H_2O (pH 7) and D_2O solvent at a peptide concentration of 10^{-6} M in the spectral range of 3100−540 cm^{-1}.

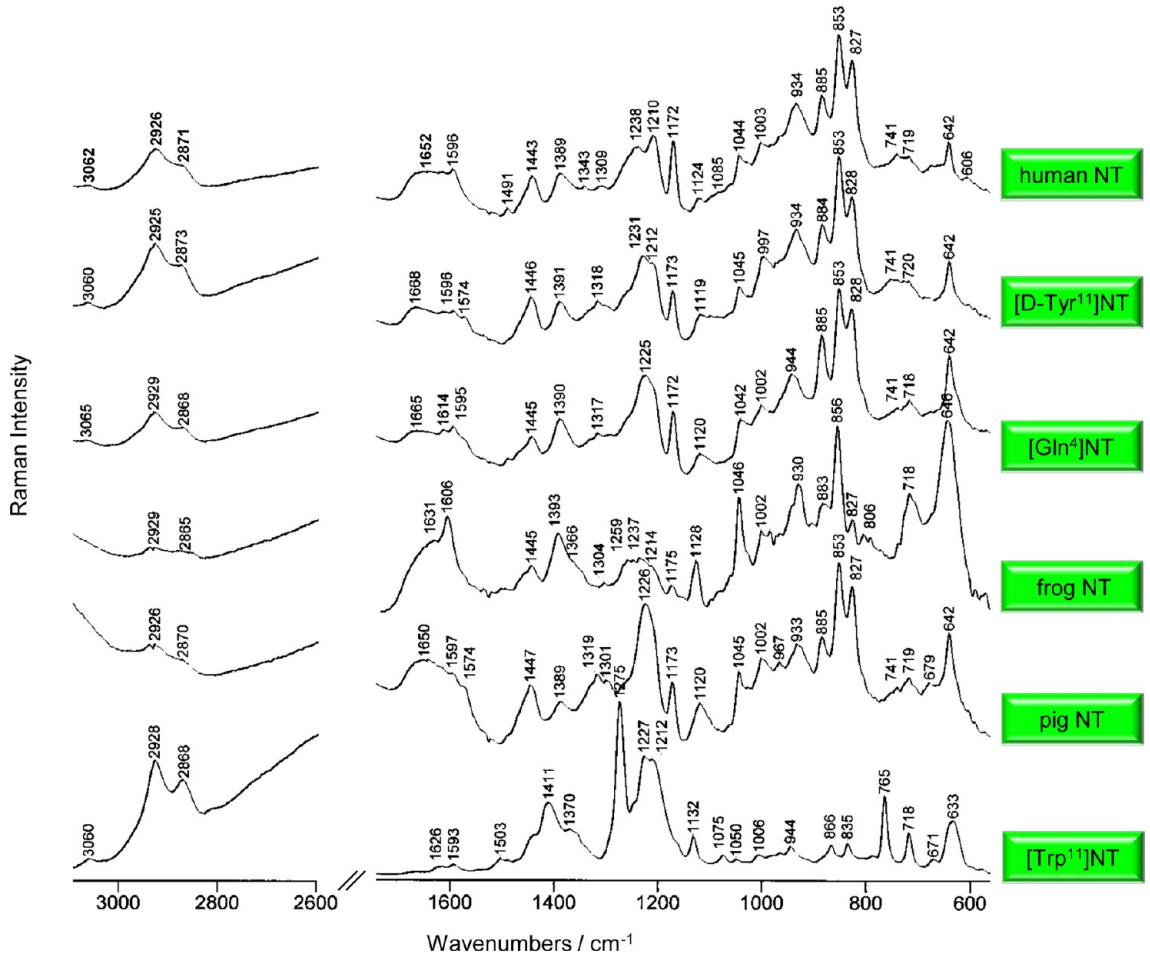

Figure 7. SERS spectra of human NT, [D-Ty^{11}]NT, pig NT, frog NT, [Gln^4]NT, and [Trp^{11}]NT in an aqueous silver sol at pH 2 and at a peptide concentration of 10^{-6} M in the spectral range of 3100−540 cm^{-1}.

dx.doi.org/10.1021/jp304205d | J. Phys. Chem. C 2012, 116, 16561−16572

direction, i.e., they increased in relative intensity with increasing pH of the solution. The asynchronous G2D correlation maps (Figure 5, parts B and D) also show the development of several cross-peaks. The appearance of these peaks suggests that the directions of the transition moments for these modes are different. The positive signs of the (934, 702), (1087, 702), and (2926, 2851) cm^{-1} peaks indicate that a pH-induced spectral change occurred earlier for the bands at 934, 1087, and 2926 cm^{-1} than for those at 702 and 2851 cm^{-1}. In contrast, the negative sign of the five cross-peaks at (1087, 934), (1389, 934), (1389, 885), (934, 885), and (1087, 885) cm^{-1} suggests that spectral alterations took place earlier for peaks at 934 and 885 cm^{-1} than for those at 1087 and 1389 cm^{-1}. Similarly, the change at 934 cm^{-1} followed that at 885 cm^{-1}. In summary, when the pH of an aqueous silver colloid became increasingly basic, first a rearrangement of the Tyr^{11} $-C_\beta C_\gamma H_2 C_\delta-$ fragment was occurred, thereby slightly strengthening the $C_\beta C_\gamma H_2 C_\delta \cdots Ag$ interaction. The strengthening of this interaction altered the contact between the $C_\beta-C_\alpha$ bond (in the $-C_\beta-C_\alpha OO^-$ group) of the Leu^{13} *C*-terminal residue and the silver colloidal substrate. Furthermore, the changes determine the improvement of the coordination of the Leu^{13} $-COO^-$ and Arg^9 $-NH_2$ groups to the substrate. During the pH change from 2 to 3, the Tyr ring that is approximately oriented horizontally moved farther from the surface, which is indicated by the decrease in the relative intensities of the Tyr modes. The subsequent increase in the alkaline reaction of the silver colloid (up to pH 11) did not alter the Tyr ring position.

In the fingerprint spectral region, the amide I and III modes for human NT immobilized onto the silver particles in an aqueous solution at pH 7 and at a peptide concentration of 10^{-6} M are expected to appear at approximately 1652 and 1238 cm^{-1}, respectively. To verify the assignment of these SERS bands, experiments in D_2O were conducted (Figure 6). As is evident from Figure 6, neither a band shift nor a difference in enhancement of the 1652 and 1238 cm^{-1} SERS signals were observed upon the H_2O/D_2O solvent exchange. This result indicates the lack of association of these bands with the amide-bond vibrations. Alternatively, these bands may be assigned to the ν(ring) + $\rho_s(NH_2)$ and ν(C−O) + δ(ring) modes, respectively, of the Tyr/Arg residues.

The influence of structural modifications, i.e., natural and synthetic mutations, on the mode of adsorption of human NT onto colloidal silver surfaces in an aqueous solution at pH 2 and at a peptide concentration of 10^{-6} M was also investigated. Figure 7 compares the SERS spectra of human, pig, and frog neurotensin, and the single-site mutants of human neurotensin, [Gln^4]NT, [Trp^{11}]NT, and [D-Tyr^{11}]NT (see Table 1). The human NT SERS spectrum under the same experimental conditions (Figure 3, middle trace) has already been discussed. This peptide was believed to interact with the silver substrate through its nearly flat Tyr^{11} ring, its deprotonated phenolic moiety, and its Leu^{13} $-C_\alpha OO^-$ group based on the presence of spectral bands that were attributed to these peptide fragments. The [D-Tyr^{11}]NT SERS spectrum exhibits bands of the same vibrations. Specifically, these bands are observed at 1596 (Y8a), approximately 1446 (Y19b + $\rho_s(C_\beta H_2)_Y$), 1389 ($\nu(C_\alpha OO^-)$), 1231 ($\nu(C-O)_Y$), 1212 (totally symmetric para-substituted benzene), 1173 ($\nu_{sym}(C_\beta C_\gamma H_2 C_\delta)$), 997, 934 ($\nu_{sym}(C_\beta-C_\alpha OO^-)_L$), 885 ($\rho_r(C_\gamma H_2)_Y$), 853/828 (Fermi doublet), 741 (ρ_b(ring)$_Y$), 720, and 642 cm^{-1} (δ(ring)$_Y$). In addition, the 1574 cm^{-1} SERS signal due to Y8b is clearly observed. Similar to human NT, the aforementioned bands are indicators of the interactions between the Tyr^{11} residue and carboxylate group of *C*-terminal Leu^{13} and the colloidal silver substrate. Other noteworthy observations include the greater enhancement of the $\nu(C-O)_Y$ band (1231 cm^{-1}) and the I_{850}/I_{830} ratio in the SERS spectrum of [D-Tyr^{11}]NT in comparison to those observed in the human NT SERS spectrum. The intensification of the 1231 cm^{-1} SERS signal is possibly due to closer interactions between the free electron pairs on the D-Tyr^{11} phenolic oxygen atom and the silver substrate. The I_{850}/I_{830} ratio in proteins ($0.30 < I_{850}/I_{830} < 2.5$) depends primarily on the state of the Tyr residue (i.e., free, hydrogen-bonded, or ionized). When the Tyr phenoxyl proton is a strong hydrogen-bond donor, the I_{850}/I_{830} ratio is equal to 0.30. However, when phenoxyl oxygen is a strong hydrogen-bond acceptor, the relative intensity ratio of the Fermi doublet increases to 2.5, whereas an I_{850}/I_{830} ratio between 1 and 1.4 indicates that the phenolic group plays the role of a donor and acceptor of moderate H-bonds. In the absence of hydrogen bonding, the relative intensity of the 850 cm^{-1} band is greatly enhanced.[52,53] As previously mentioned, the I_{850}/I_{830} ratio increased from 1.2 for human NT to 1.43 for its [D-Tyr^{11}]NT single-modified analogue, which suggests a slight weakening of the Tyr hydrogen bonding upon change of the Tyr^{11} conformation (L → D). Furthermore, the enhancement of the 1665 and 1574 cm^{-1} spectral features agrees with the model for $TyrO^-\cdots Ag$ interaction proposed by Bjerneld and co-workers.[43]

The SERS spectra of pig NT and [Gln^4]NT in the silver sol exhibited approximately the same vibrational patterns as that of [D-Tyr^{11}]NT. However, two differences were obvious. The first difference is associated with the characteristic stretching mode of the phenolic C−O bond (1225 cm^{-1}), which increased in intensity and practically dominated the spectrum of [Gln^4]NT. This increased intensity could be explained on the basis of the increased contact between the free electron pairs on the phenolic oxygen and the silver substrate (enhanced in the following order: human NT < [D-Tyr^{11}] < pig NT < [Gln^4]NT). Thus, based on the observation that L-serine (Ser^7) produced greater spectral changes than did the substitution of L-glutamic acid at the 4 position (Glu^4) with L-glutamine (Gln^4), chain modification at the 7 position in the amino acid sequence of human NT apparently is important. This finding supports the earlier conclusion about the importance of the *C*-terminal peptide fragment in the interaction with the silver substrate. The second difference is connected to the I_{850}/I_{830} ratio for pig NT and [Gln^4]NT being equal to 1.2, which is similar to the I_{850}/I_{830} ratio for human NT. This observation provides evidence that the previously discussed single-site modifications of the human NT did not alter the hydrogen bonding of the phenolic group in human NT. The applied modifications also did not change the overall pattern of the Tyr modes. Therefore, we concluded that the Tyr^{11} ring in [D-Tyr^{11}]NT, [Gln^4]NT, and pig NT interacts with the silver substrate in the same manner as that in human NT.

Large spectroscopic changes are observed for frog NT (see Table 1) in comparison to human and pig NT and the [D-Tyr^{11}]NT and [Gln^4]NT analogues. For this five-sites modified peptide (Leu^2 → Ser^2, Tyr^3 → His^3, Glu^4 → Ile^4, Asn^5 → Ser^5, and Pro^7 → Ala^7), the lower-wavenumber band of the Fermi doublet lost most of its intensity (I_{850}/I_{830} = 5). This loss of intensity indicates the presence of a non-hydrogen-bonded phenolic group. The position of Y8a (1606 cm^{-1}) suggests the presence of a protonated phenolic group in the frog NT,

dx.doi.org/10.1021/jp304205d | J. Phys. Chem. C 2012, 116, 16561−16572

whereas the decrease in the relative intensity of the ν(C−O) mode (1237 cm^{-1}) implies that the pair of free electrons on this group only assists in the interaction with the silver surface. In contrast, the 1048 and 640 cm^{-1} SERS bands gained relative intensity. The former band is assigned to ν(C−C) and/or $\rho_r(C_\gamma H_2)_Y$. The latter band is due to the Tyr^{11} ring bending mode. The high value of the full-width-at-half-maximum (fwhm) for the 640 cm^{-1} band (fwhm = 45 cm^{-1}) that overlaps with the amide IV mode is mainly due to in- and out-of-plane deformations of strongly coupled amino groups. This assignment is supported by the appearance of two new SERS signals, due to amide I and III vibrations at 1631 and 1259 cm^{-1}, respectively. Thus, the amide mode moved closer to the silver surface and improved the signal from the amide bands in the frog NT SERS spectrum.

In the SERS spectrum of the [Trp^{11}]NT analogue (Figure 6) in which the L-tryptophane residue is located at the 11 position of the NT amino acid sequence (Trp^{11}) instead of Tyr^{11}, bands due to Trp^{11} were enhanced almost exclusively, which suggests that peptide interaction occurs through this residue. The enhanced bands include those at 1593, 1503, 1439, 1370, 1227, 1212, 1006, and 765 cm^{-1} (see Table 2 for band assignments). Among these bands, the 1227, 1212, and 765 cm^{-1} bands due to the $\nu(C_3-C_{10})$, the totally symmetric ring stretch of the phenyl co-ring, and the symmetric co-pyrrole in-plane ring breathing modes, respectively, were moderately enhanced. These findings, together with the low relative intensity, width widening (Δ_{fwhm} = +7 cm^{-1}), and downshift in wavenumber (by 4 cm^{-1}) of the 1006 cm^{-1} band (W16) in comparison with those of the corresponding Raman band,[30] may suggest an approximately horizontal position of the Trp^{11} ring on the colloidal silver surface. The 1370 and 1439 cm^{-1} SERS signals related to the copyrrole $-C_8-N_1H-C_2-$ unit vibrations also imply an orientation of the indole ring that allows the free electron pair on the nitrogen atom to interact with the silver nanoparticles. This conclusion is supported by the 1132 cm^{-1} spectral feature that is due to the $\delta(N_1H)$ mode. However, this orientation should limit the contact between the $-C_2=C_3-$ unit and the silver colloidal surface (i.e., the 1549 cm^{-1} band was negligibly enhanced).

The strongest [Trp^{11}]NT SERS signal at 1275 cm^{-1} and a 633 cm^{-1} band arise from the in-phase combination of the NH bending and the CN stretching (amide III) and NH out-of-plane bending (amide V) modes of the peptide bond, respectively. Two other bands at 1411 and 944 cm^{-1} are characteristic of the carboxylate-group vibrations (see Table 2 for detailed band assignments). Therefore, the N−H unit of the −CONH− bond (strongly) and the $-COO^-$ of Leu^{13} interact with the silver nanoparticles.

CONCLUSIONS

The adsorption mode of NT in an aqueous solution of colloidal silver particles with diameters of 20 − 25 nm and the changes of this mode, which are influenced by different excitation wavelengths (488.0, 514.5, and 785.0 nm), peptide concentrations (10^{-4}–10^{-6} M), pH levels of the solutions (from pH 2 to 11), and H_2O/D_2O solvent exchange characteristics, were determined. The type of amino acid modification responsible for a significant increase/decrease in NT physiological function that causes an alteration of the peptide−silver colloidal surface interaction was also investigated. By observing the SERS spectral profiles, we made the following conclusions:

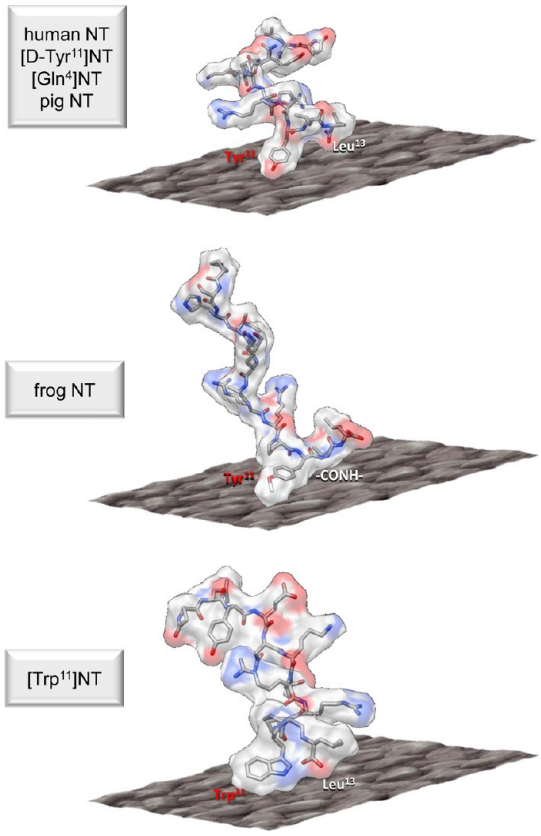

Figure 8. Possible mode for the investigated peptides interaction with the colloidal silver surface at a peptides concentration of 10^{-6} M.

(a) The deposited NT exhibited a sponge-like structure with a width/length in the range of 40−90 nm and covered the large assemblies on the substrate surface with a random distribution.

(b) The relative intensities of the bands in these spectra strongly depend on the excitation wavelength.

(c) The NT concentration of 10^{-4} M was the optimal peptide concentration for monolayer colloidal coverage.

(d) NT is adsorbed through the Tyr residue and the carboxylate group onto the colloidal silver surface in an aqueous solution at pH 2 and at a peptide concentration of 10^{-6} M.

(e) The SERS spectrum at a peptide concentration of 10^{-5} M (Figure 3, middle trace) indicates that both the carboxylate and amino groups are in close proximity to the silver surface.

(f) At a NT concentration of 10^{-4} M, aside from the Tyr ring oriented vertically, the $-NH_2$ group interacts with the colloidal silver surface. Decreases in the NT concentration caused the Tyr ring to lean down onto this surface. The growth of the silver surface coverage by the nearly flat-oriented Tyr rings limits the interaction between the amine group of Arg and the silver surface, whereas it promotes the $-C_\alpha OO^-$ group adsorption onto the silver surface.

(g) Upon an increase in the pH of the solution from 2 to 3, the Tyr ring moved farther from the silver colloidal surface. A further increase of the alkaline reaction of the silver colloid (up to 11) did not alter the Tyr ring position.

(h) The Tyr^{11} → D-Tyr^{11} substitution caused a closer interaction between the free electron pairs on the D-Tyr^{11} phenolic oxygen atom and the silver substrate and slightly weaker hydrogen bonding for the tyrosine residue.

(i) The chain modification at the 4 position in the amino acid sequence of human NT occurred in the form of L-glutamine

dx.doi.org/10.1021/jp304205d | J. Phys. Chem. C 2012, 116, 16561−16572

(Gln^4) produced smaller spectral changes (i.e., it did not alter the hydrogen bonding of the phenolic group) than did the $Pro^7 \rightarrow Ser^7$ replacement.

(j) Non-hydrogen-bonded protonated phenolic is present in the frog NT.

(k) The replacement of Tyr^{11} with Trp^{11} caused a dramatic change in the SERS spectra.

Figure 8 presents a possible mode for the investigated peptides interaction with the colloidal silver surface.

AUTHOR INFORMATION

Corresponding Author

*E-mail: podstawk@chemia.uj.edu.pl. Tel: +48-12-663-2077. Fax: +48-12-634-0515.

Notes

The authors declare no competing financial interest.

ACKNOWLEDGMENTS

This work was supported by the National Science Center of the Polish Ministry of Science and Higher Education (Grant No. N N204 159136 to E.P.). Y.K. gratefully acknowledges the financial support of HUFS.

REFERENCES

(1) Carraway, R.; Leeman, S. E. *J. Biol. Chem.* **1973**, *248*, 6854−6861.
(2) Carraway, R.; Leeman, S. E. *J. Biol. Chem.* **1975**, *250*, 1907−1911.
(3) Martin, S.; Botto, J.-M.; Vincent, J.-P.; Mazella, J. *Mol. Pharmacol.* **1999**, *55*, 210−215.
(4) Thomas, R. P.; Hellmich, M. R.; Townsend, C. M., Jr.; Evers, B. M. *Endocr. Rev.* **2003**, *24*, 571−599.
(5) Alshoukr, F.; Rosant, C.; Maes, V.; Abdelhak, J.; Raguin, O.; Burg, S.; Sarda, L.; Barbet, J.; Tourwé, D.; Pelaprat, D.; Gruaz-Guyon, A. *Bioconjugate Chem.* **2009**, *20*, 1602−1610.
(6) Myers, R. A.; Shearman, M.; Kitching, M. O.; Ramos-Montoya, A.; Neal, D. E.; Ley, S. V. *Chem. Biol.* **2009**, *4*, 503−525.
(7) Reubi, J. C.; Waser, B.; Friess, H.; Buchler, M.; Laissue, J. *Gut* **1998**, *42*, 546−550.
(8) Souaze, F.; Dupouy, S.; Viardot-Foucault, V.; Bruyneel, E.; Attoub, S.; Gespach, C.; Gompel, A.; Forgez, P. *Cancer Res.* **2006**, *66*, 6243−6249.
(9) Cusack, B.; McCormick, D. J.; Pang, Y.-P.; Souder, T.; Garcia, R.; Fauq, A.; Richelson, E. *J. Biol. Chem.* **1995**, *270*, 18359−18366.
(10) St-Pierre, S.; Lalonde, J. M.; Gendreau, M.; Quirion, R.; Regoli, D.; Rioux, F. *J. Med. Chem.* **1981**, *24*, 370−376.
(11) Chakravarty, P. K.; Ransom, R. W. *Curr. Pharm. Des.* **1995**, *1*, 317−324.
(12) Orwig, K. S.; Lassetter, M. R.; Hadden, M. K.; Dix, T. A. *J. Med. Chem.* **2009**, *52*, 1803−1813.
(13) Hong, F.; Cusack, B.; Fauq, A.; Richelson, E. *Curr. Med. Chem.* **1997**, *4*, 421−434.
(14) Granier, C.; van Rietschoten, J.; Kitabgi, P.; Poustis, C.; Freychet, P. *Eur. J. Biochem.* **1982**, *124*, 117−125.
(15) Tanaka, K.; Masu, M.; Nakanishi, S. *Neuron* **1990**, *4*, 847−854.
(16) Carraway, R. E.; Leeman, S. E. In *Peptides: Chemistry, Structure and Biology*; Walter, R., Meinhofer, J., Eds.; Ann Arbor Science: Ann Arbor, MI, 1975; pp 679−685.
(17) Lazarus, L. H.; Perrin, M. H.; Brown, M. R. *J. Biol. Chem.* **1997**, *252*, 7174−7179.
(18) Quirion, R.; Regoli, D.; Rioux, F.; St-Pierre, S. *Br. J. Pharmacol.* **1980**, *69*, 689−692.
(19) Loosen, P. T.; Nemeroff, C. B.; Bissette, G.; Burnett, G. B.; Prange, A. J.; Lipton, M. A. *Neuropharmacology* **1978**, *17*, 109−113.
(20) Podstawka, E. *Biopolymers* **2008**, *89*, 506−521.
(21) Podstawka, E. *J. Raman Spectrosc.* **2008**, *39*, 1290−1305.
(22) Podstawka, E.; Niaura, G. *J. Phys. Chem. B* **2009**, *113*, 10974−10983.
(23) Podstawka, E.; Niaura, G.; Proniewicz, L. M. *J. Phys. Chem. B.* **2010**, *114*, 1010−1029.
(24) Podstawka, E.; Niaura, G.; Proniewicz, L. M. *J. Phys. Chem. B* **2010**, *114*, 5117−5124.
(25) Podstawka, E. *Biopolymers* **2008**, *89*, 980−992.
(26) Podstawka, E.; Ozaki, Y.; Proniewicz, L. M. *Langmuir* **2008**, *24*, 10807−10816.
(27) Ignatjev, I.; Podstawka-Proniewicz, E.; Niaura, G.; Lombardi, J.; Proniewicz, L. M. *J. Phys. Chem. B* **2011**, *115*, 10525−10536.
(28) Podstawka-Proniewicz, E.; Ignatjev, I.; Niaura, G.; Proniewicz, L. M. *J. Phys. Chem. C* **2012**, *116*, 4819−4200.
(29) Coy, D. H.; Heinz-Erian, P.; Jiang, N. Y.; Sasaki, Y.; Taylor, J.; Moreau, J. P.; Wolfrey, W. T.; Gardner, J. D.; Jensen, R. T. *J. Biol. Chem.* **1988**, *263*, 5056−5060.
(30) Podstawka-Proniewicz, E.; Kudelski, A.; Kim, Y.; Proniewicz, L. M. *J. Phys. Chem. B* **2011**, *115*, 6709−6721.
(31) Podstawka-Proniewicz, E.; Kudelski, A.; Kim, Y.; Proniewicz, L. M. *J. Phys. Chem. B* **2011**, *115*, 7097−7108.
(32) Podstawka-Proniewicz, E.; Kudelski, A.; Kim, Y.; Proniewicz, L. M. *J. Raman Spectrosc.* **2012**, in press.
(33) Lee, P. C.; Meisel, D. *J. Phys. Chem.* **1982**, *86*, 3391−3395.
(34) Hayashi, S.; Koga, R.; Ohtuji, M.; Yamamoto, K.; Fujii, M. *Solid State Commun.* **1990**, *76*, 1067−1070.
(35) Lombardi, J. R.; Birke, R. L. *J. Phys. Chem. C* **2008**, *112*, 5605−5617.
(36) Ahern, A.; Garrell, R. L. *Langmuir* **1991**, *7*, 254−261.
(37) Whittaker, M. M.; DeVitos, V. L.; Asher, S. A.; Whittaker, J. W. *J. Biol. Chem.* **1989**, *264*, 7104−7106.
(38) MacDonald, G. M.; Bixby, K. A.; Barry, B. A. *Proc. Natl. Acad. Sci. U.S.A.* **1993**, *90*, 11024−11028.
(39) Jakobsen, R. J.; Brewer. *Appl. Spectrosc.* **1962**, *16*, 32−35.
(40) Grace, L. I.; Cohen, R.; Dunn, T. M.; Lubman, D. M.; de Vries, M. S. *J. Mol. Spectrosc.* **2002**, *215*, 204−219.
(41) Johnson, C. R.; Ludwig, M.; Asher, S. A. *J. Am. Chem. Soc.* **1986**, *108*, 905−912.
(42) Tripathi, G. N. R.; Schuler, R. H. *J. Chem. Phys.* **1984**, *81*, 113−121.
(43) Bjerneld, E. J.; Johansoon, P.; Käll, M. *Single Mol.* **2000**, *3*, 239−248.
(44) Faulds, K.; Littleford, R. E.; Graham, D.; Dent, G.; Smith, W. E. *Anal. Chem.* **2004**, *76*, 592−598.
(45) Stern, D. A.; Salaita, G. N.; Lu, F.; McCargar, J. W.; Batina, N.; Frank, D. G.; Laguren-Davidson, L.; Lin, Ch.-H.; Walton, N.; Gui, J. Y.; Hubbard, A. T. *Langmuir* **1988**, *4*, 711−722.
(46) Hellwig, P.; Pfitzner, U.; Behr, J.; Rost, B.; Pesavento, R. P.; v. Donk, W.; Gennis, R. B.; Michel, H.; Ludwig, B.; Mantele, W. *Biochemistry* **2002**, *41*, 9116−9125.
(47) Rava, R. P.; Spiro, T. G. *J. Am. Chem. Soc.* **1984**, *106*, 4062−4064.
(48) Luca, S.; White, J. F.; Sohal, A. K.; Filippov, D. V.; van Boom, J. H.; Grisshammer, R.; Baldus, M. *Proc. Natl. Acad. Sci. U.S.A.* **2003**, *100*, 10706−10711.
(49) Noda, I. *Vib. Spectrosc.* **2004**, *36*, 143−165.
(50) Noda, I. *Handbook of vibrational spectroscopy*; Chalmes, J. M., Griffiths, P. R., Eds.; John Wiley & Sons: Chichester, UK, 2002.
(51) Noda, I.; Ozaki, Y. *Two-Dimensional Correlation Spectroscopy: Applications in Vibrational and Optical Spectroscopy*; Wiley & Sons: Chichester, UK, 2002.
(52) Siamwiza, M. N.; Lord, R. C.; Chen, M. C. *Biochemistry* **1975**, *14*, 4870−4876.
(53) Arp, Z.; Autrey, D.; Laane, J.; Overman, S. A.; Thomas, G. J., Jr. *Biochemistry* **2001**, *40*, 2522−2529.